



Solvent induced supramolecular polymorphism in Cu(II) coordination complex built from 1,2,4-triazolo[1,5-*a*]pyrimidine: Crystal structures and anti-oxidant activity

Karim Chkirate^a, Saad Fettach^b, Mohamed El Hafi^a, Khalid Karrouchi^c, Bouchaib Elotmani^a, Joel T. Mague^d, Smaail Radi^e, My El Abbes Faouzi^b, N.N. Adarsh^f, El Mokhtar Essassi^a, Yann Garcia^{f,*}

^a LCOH, Département de Chimie, Faculté des Sciences, Université Mohamed V, BP1014, Rabat 10100, Morocco

^b Biopharmaceutical and Toxicological Analysis Research Team, Laboratory of Pharmacology and Toxicology, Pharmacokinetic Research Team, Faculty of Medicine and Pharmacy, University Mohammed V of Rabat, Morocco

^c Laboratory of Analytical Chemistry and Bromatology, Faculty of Medicine and Pharmacy, Mohamed V University, Rabat, Morocco

^d Department of Chemistry, Tulane University, New Orleans, LA 70118, USA

^e LCAE, Département de Chimie, Faculté des Sciences, Université Mohamed I, BP 524, 60 000 Oujda, Morocco

^f Institute of Condensed Matter and Nanosciences, Molecular Chemistry, Materials and Catalysis (IMCN/MOST), Université catholique de Louvain, Place L. Pasteur 1, 1348 Louvain-la-Neuve, Belgium

ARTICLE INFO

Keywords:

Coordination polymer
Triazole
Pyrimidine
Supramolecular isomerism
Antioxidant property

ABSTRACT

Two Cu(II) coordination complexes, **C1** and **C2** of the formula $[\text{Cu}(\text{L})_2(\text{H}_2\text{O})_2]$, have been prepared by reaction between $\text{CuCl}_2 \cdot 2\text{H}_2\text{O}$ and 7-ethoxycarbonylmethyl-5-methyl-1,2,4[1,5-*a*]pyrimidine (**L**) in a 1:2 M:L molar ratio. The **L** molecule decomposes during the reaction process into 7-carboxy-5-methyl-[1,2,4]-triazolo[1,5-*a*]pyrimidine (**4**) through an intermediate, ethyl 2,2-dihydroxy-2-(5-methyl-[1,2,4]triazolo[1,5-*a*]pyrimidin-7-yl)acetate (**5**), which has been isolated and its crystal structure determined by X-ray diffraction. The X-ray analysis of the single crystals of $[\text{Cu}(\text{L})_2(\text{H}_2\text{O})_2]$ obtained from the slow evaporation of EtOH and MeOH, separately, revealed the formation of “solvent induced” polymorphs **C1** and **C2**, respectively. The primary supramolecular synthon for **C1** and **C2** are six membered ring, and square shaped hydrogen bonded architecture, respectively. The self-assembly of such synthons resulted in a two dimensional hydrogen bonded sheet supported by O–H...O interactions. In addition, the antioxidant properties of the ligands and its complexes were evaluated in vitro using 1,1-diphenyl-2-picrylhydrazyl acid, 2,2'-azino-bis (3-ethylbenzothiazoline-6 sulfonic acid radical scavenging methods and ferric reducing antioxidant power.

1. Introduction

Reactive oxygen species (ROS) are natural by products of cellular oxidative metabolism and play important roles in the modulation of cell survival, cell death, differentiation, cell signalling, and inflammation-related factor production. However, the excess production of ROS can become toxic to the major components of the cell, lipids, proteins and nucleic acids, and gives rise to the oxidative stress that will be involved in various pathologies [1–3].

Antioxidant pharmacotherapy has appear as a tool to minimize the bimolecular damage caused by the attack of ROS to these vital constituents of living organisms, and therefore synthetic antioxidants have received much attention from the pharmaceutical viewpoint [3].

However, a significant number of research teams have concentrated on the role of complexes as antioxidants [4–6].

The chemistry of 1,2,4-triazolo[1,5-*a*]pyrimidine has grown rapidly due to their biological activities and rich coordination chemistry [7,8]. Such molecules and their derivatives exhibit biological activity in various therapeutic domains of importance such as anti-cancer [9], anti-viral [10–12], anti-malarial [13], anti-parasitic [14], anti-leishmania [15], anti-microbial [16,17], anti-inflammatory [18], and hypoglycemic [19]. Their structure is similar to that of purine and adenine. Their condensed ring system is distinguished by the fact that the pyrimidine nitrogen atom is at the bridgehead with the disappearance of the acid proton from the five-membered ring [20,21]. 1,2,4-Triazolo [1,5-*a*]pyrimidine can be used to study metal-ligand interactions

* Corresponding author.

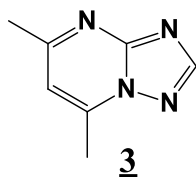
E-mail address: yann.garcia@uclouvain.be (Y. Garcia).

<https://doi.org/10.1016/j.jinorgbio.2020.111092>

Received 20 June 2019; Received in revised form 17 April 2020; Accepted 18 April 2020

Available online 05 May 2020

0162-0134/ © 2020 Elsevier Inc. All rights reserved.



Scheme 1. 5,7-Dimethyl-1,2,4-triazolo[1,5-*a*]pyrimidine.

similar to those observed in biological systems. In addition to their rich coordination chemistry, the properties of 1,2,4-triazolo[1,5-*a*]pyrimidines have aroused the interest of these compounds [22–25].

Our strategy was to develop a simple, high-yield, synthetic procedure in a few steps to prepare acetamide derivatives [26–28]. The literature shows that 5,7-dimethyl-1,2,4-triazolo[1,5-*a*]pyrimidine (**3**) has been described as a ligand of interest for heavy metal complexes [29–34], involving exclusively the nitrogen atom at position 3 of the bicyclic system (Scheme 1).

The aim of this work was to investigate the influence of the ethoxycarbonyl methyl group at position 7 of the 1,2,4-triazolopyrimidine unit by designing 2-(5-methyl-[1,2,4]triazolo[1,5-*a*]pyrimidin-7-yl)acetate (**L**) prepared from reaction of 3-amino-1,2,4-triazole (**1**) and 4-hydroxy-6-methyl-2-pyrone (Scheme 2).

In consideration of the above-mentioned findings, and as a continuation of our efforts to identify new heterocyclic compound and coordination complexes [35–41], we report herein solvent dependent synthesis of supramolecular polymorphs of a novel Cu(II) coordination complex with 1,2,4-triazolo[1,5-*a*]pyrimidine and their *in vitro* anti-oxidant activities.

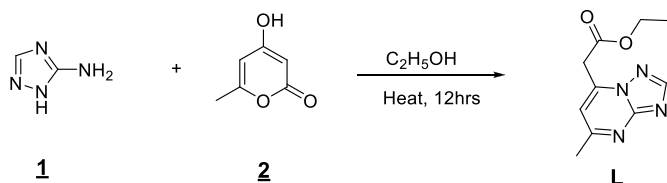
2. Results and discussion

2.1. Synthesis

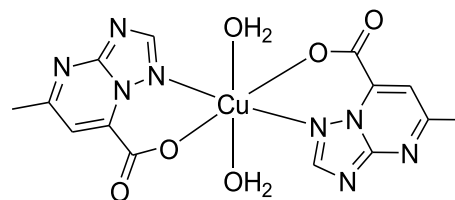
Reaction of $\text{CuCl}_2 \cdot 2\text{H}_2\text{O}$ dissolved in ethanol with **L** in hot ethanol, afforded single crystals of $[\text{Cu}(\mathbf{4})_2(\text{H}_2\text{O})_2]$ ($\mathbf{4}$ = 7-carboxy-5-methyl-[1,2,4]-triazolo[1,5-*a*]pyrimidine), which crystallizes in the monoclinic system according to X-ray diffraction. In addition, reaction of $\text{CuCl}_2 \cdot 2\text{H}_2\text{O}$ in the presence of $\text{FeCl}_2 \cdot 4\text{H}_2\text{O}$ dissolved in hot methanol afforded single crystal of the same formula, $[\text{Cu}(\mathbf{4})_2(\text{H}_2\text{O})_2]$, but which crystallizes in the triclinic system, thus identifying polymorphs (Scheme 3). Surprisingly, during the complexation reaction, the ethoxycarbonyl group of 1,2,4-triazolo[1,5-*a*]pyrimidine, was transformed under the operating conditions, into a carboxyl group, giving rise to a new molecule 7-carboxy-5-methyl-[1,2,4]-triazolo[1,5-*a*]pyrimidine (**4**), which is included in the crystal structure of the complexes as a ligand (Scheme 3). The complexes were characterized by electrospray ionization mass spectrometry (ESI-MS), high resolution mass spectrometry (HRMS), FT-IR spectroscopy, UV–vis spectroscopy and single crystal X-ray diffraction (see next sections).

A possible mechanism can be proposed to explain the formation of ligand **4**.

The initial step of the reaction corresponds to an oxidation reaction by air oxygen of the methylene group belonging to the ethoxycarbonylmethyl group, leading to the intermediate [A], as shown in Scheme 4. The ester function of [A] undergoes a hydrolysis reaction,



Scheme 2. Synthesis of **L**.



Scheme 3. Molecular structure of $[\text{Cu}(\mathbf{4})_2(\text{H}_2\text{O})_2]$ (**C1** and **C2**).

which is followed by a decarboxylation reaction of the α -keto acid [B], giving rise to an aldehyde [C], which after an oxidation reaction, leads to 1,2,4-triazolo[1,5-*a*]pyrimidine carboxylic acid **4**. The later reacts with $\text{CuCl}_2 \cdot 2\text{H}_2\text{O}$ to give $[\text{Cu}(\mathbf{4})_2(\text{H}_2\text{O})_2]$ (Scheme 4).

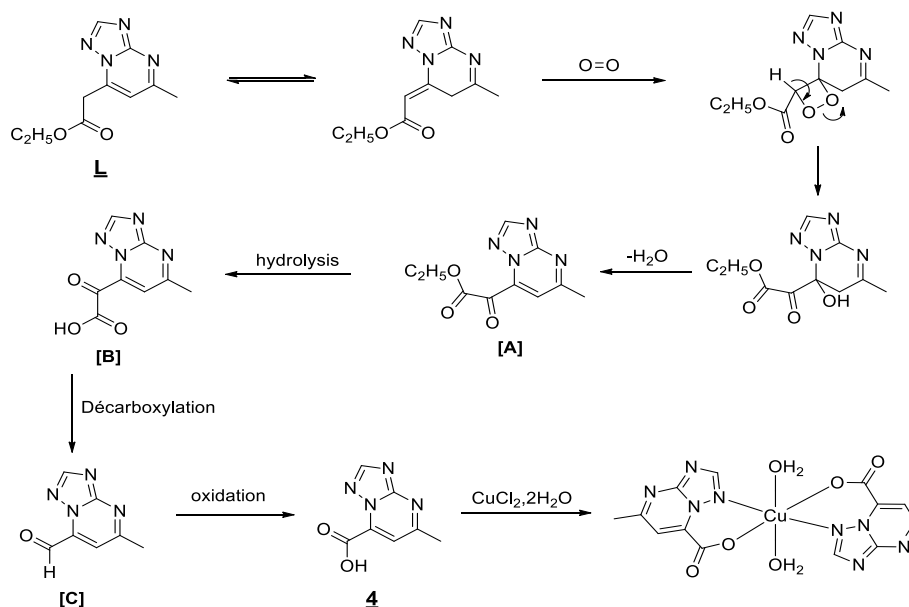
It should be noted that in this type of reaction, the driving force of the rearrangement corresponds to the oxidation reaction, making it possible to convert the methylene group in α -position of the ester function into a carbonyl group and leading to α -ketoester [A] [42–44]. Therefore, it seemed to us necessary to isolate this last compound to confirm its intermediary role. Interestingly, the action of $\text{MnCl}_2 \cdot 4\text{H}_2\text{O}$ dissolved in ethanol on 1,2,4-triazolo[1,5-*a*]pyrimidine (**L**) in hot ethanol, allowed us to isolate single crystals of which X-ray diffraction analysis shows that it is the hydrate corresponding to the compound [A] (Scheme 4), namely ethyl 2,2-dihydroxy-2-(5-methyl-[1,2,4]triazolo[1,5-*a*]pyrimidin-7-yl)acetate quoted as **5** hereafter (Scheme 5). This result is of great importance in organic chemistry, since it is well established that hydrates of ketones are not stable, unlike the only hydrate of chloral [45].

2.2. FT-IR spectroscopy

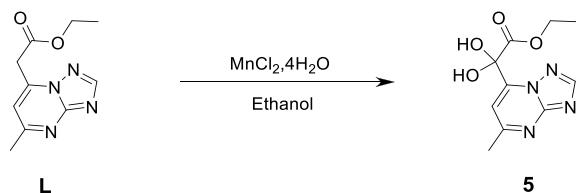
The solid state analyses of **L** and their metal complexes **C1** and **C2** were performed using Fourier Transform infrared (IR) spectroscopy. FT-IR spectra were recorded from 4000 to 400 cm^{-1} , and the main characteristic stretching frequencies and their corresponding interpretation are shown in Table S1 (Appendix A). An overlay of the IR spectra of **L**, **C1** and **C2** along with their structures is illustrated in Figs. S1 and S2 (Appendix A). The ligand contains coordination active groups such 1,2,4-triazole, and thiourea, which could coordinate to the metal ions. To assign the IR bands, the ligand spectrum was carefully compared with that of the complexes **C1** and **C2**. It could be deduced that, the band at 3065 cm^{-1} is attributed to the C–H stretching vibrations of the aromatic ring. The bands between 2915 and 2990 cm^{-1} were assigned to the symmetrical and asymmetric stretching vibrations of CH_3 and CH_2 . These bands have disappeared in the spectra of the complexes. The carbonyl ($\text{C}=\text{O}$) and azomethine ($\text{C}=\text{N}$) bands appear in the ligand spectrum around 1735 and 1630 cm^{-1} , respectively. These stretching frequencies shifted towards 1653 and 1607 cm^{-1} in the spectra of the complexes. In the FT-IR, the peaks of the samples **C1** and **C2**, at 513 and 405 cm^{-1} , indicated the presence of stretching vibrations $\nu(\text{Cu}-\text{O})$ and $\nu(\text{Cu}-\text{N})$, which belongs to the $\text{Cu}(\text{II})-\text{O}$ and $\text{Cu}(\text{II})-\text{N}$, respectively. These two characteristic peaks were absent in the FT-IR spectra of the free ligand **L**.

2.3. UV–visible spectroscopy

The electronic absorption spectral data for the ligand and its complexes were recorded at room temperature in the $\lambda = 200\text{--}900$ nm range using DMSO. UV–vis spectra of **L** showed two absorption bands, one at $\lambda_{\text{max}} = 294$ nm and a broad band in the 310–380 nm range with $\lambda_{\text{max}} = 340$ nm (Fig. S3, Appendix A). The absorption band observed at $\lambda_{\text{max}} = 294$ nm is attributed to the $\pi-\pi^*$ of aromatic rings. The other band observed at $\lambda_{\text{max}} = 340$ nm is assigned to $n-\pi^*$ of azomethine and $\text{C}=\text{S}$ groups. In the electronic absorption of the $\text{Cu}(\text{II})$ complexes **C1** and **C2**, the absorption band found at $\lambda_{\text{max}} = 294$ nm is due to the $n-\pi^*$ transitions. Indeed, the UV–vis spectra show the disappearance of the



Scheme 4. Mechanism proposed to explain the formation of the ligand 4.



Scheme 5. Isolation of the intermediate product 5.

absorption band at $\lambda_{\text{max}} = 340$ nm observed in the ligand L.

2.4. Single crystal structures of 5, C1 and C2

2.4.1. Ethyl 2,2-dihydroxy-2-(5-methyl-[1,2,4]triazolo[1,5-a]pyrimidin-7-yl)acetate (5)

The intermediate molecule 5, crystallizes in the centrosymmetric space group $P\bar{1}$ (Table 1). The asymmetric unit contains two crystallographically independent molecules of 5, and four such molecules were present in the unit cell. The triazole-pyrimidine ring and the ester function of each crystallographically independent molecules of 5, showed torsion angles of 68.74° and 71.11° . In the crystal structure, the geminal diol showed hydrogen bonding with the N atoms of the 1,2,4-triazole and pyrimidine via $O-H\cdots N$ interactions [$O-H\cdots N = 2.782(2)$ – $2.894(2)$ Å, $\angle O-H-N = 164(2)$ – $172.9(19)^\circ$]. Such supramolecular interactions resulted in a 1D hydrogen bonded chain, involving alternate packing of crystallographically independent molecules of 5. The 1D chains are further packed in a parallel fashion displaying interdigitation of ester functions supported by various supramolecular weak interactions (Fig. 1).

2.4.2. $[Cu(4)_2(H_2O)_2]$ (C1)

Single crystals of C1 were grown from EtOH solvent at r.t. and crystallized in centrosymmetric monoclinic $P2_1/n$ space group (Table 1). The asymmetric unit contains one Cu atom, one molecule of ligand (4), and one molecule of water (both water and ligand are coordinated to the metal centre). The Cu atom is located on centre of inversion symmetry, so that the rest of the complex is generated by the symmetry operation. There are such four molecules of Cu(II) coordination complexes present in the unit cell, in which all the adjacent molecules were symmetry related by a 2-fold screw axis and a n' glide

plane. The Cu(II) metal centre displayed a distorted octahedral geometry [$\angle N-Cu-O = 85.90(6)$ – $94.10(6)^\circ$; $\angle O-Cu-O = 84.77(6)$ – $95.23(6)^\circ$] wherein the equatorial positions were occupied by the nitrogen atom (1,2,4-triazole) and a O atom (carboxylate) of two molecules of ligand 4; the apical positions were coordinated by the water molecules. The metal coordinated ligand (4) is almost planar; the torsion angle between the aromatic ring (1,2,4-triazole and pyrimidine), and the carboxylate functionality is $\sim 6.48^\circ$. The dipositive charge of Cu(II) metal centre is balanced by two molecules of mono-negatively charged carboxylate ion of the ligand (4). The Cu(II)–O and Cu(II)–N bond distances in C1 are comparable to those in Cu(II) complexes of reported carboxylate-triazole ligand [46,47]. Interestingly, each complex molecule undergo supramolecular interactions with six other molecules; the two metal bound water molecules participate in bifurcated hydrogen bonding with N atom and O atoms of pyrimidine and carboxylate functions of the ligand via $O-H\cdots O$ and $O-H\cdots N$ interactions [$O-H\cdots O = 2.868(2)$ Å, $\angle O-H-O = 165.37(18)^\circ$; $O-H\cdots N = 2.924(2)$ Å, $\angle O-H-N = 173.2(2)^\circ$] (Table 2).

Thus, the hydrogen bonding involving six membered molecules and the molecule present in the centre of this six membered ring, formed the primary supramolecular synthon. The extended coordination of these synthon, resulted in a 2D hydrogen bonded network structure. The 2D hydrogen bonded architectures are further packed on top of each other via weak $C-H\cdots O$ hydrogen bonding interaction, participated by the C–H of the methyl and O atom of the carboxylate functionalities present in the ligand [$C-H\cdots O = 3.422(3)$ Å, $\angle C-H-O = 163.4(8)^\circ$] (Fig. 2).

2.4.3. $[Cu(4)_2(H_2O)_2]$ (C2)

Interestingly, the Cu(II) coordination complex including 4, in the presence of the MeOH crystallized in the centrosymmetric triclinic space group $P\bar{1}$ (Table 1). Basically, the Cu(II) coordination complexes C1 and C2 are polymorphs, crystallizing in two different space groups, namely monoclinic $P2_1/n$ and triclinic $P\bar{1}$, respectively. The asymmetric unit consists of one Cu atom, one molecule of ligand (4), and one molecule of water (both water and ligand are coordinated to the metal centre). The crystallographic inversion centre is located on the Cu(II) metal centre. Due to the presence of this symmetry, another half of the complex is generated by this symmetry operation. In contrast to complex C1, there was only one molecule of Cu(II) coordination complex

Table 1
Crystallographic and refinement data for **5**, **C1** and **C2**.

| | 5 | C1 | C2 |
|--|---|---|---|
| CCDC number | 1915469 | 1915467 | 1915468 |
| Empirical formula | C ₁₀ H ₁₂ N ₄ O ₄ | C ₁₄ H ₁₄ CuN ₈ O ₆ | C ₁₄ H ₁₄ CuN ₈ O ₆ |
| Formula weight | 252.24 | 453.86 | 453.87 |
| Crystal size (mm) | 0.36 × 0.32 × 0.15 | 0.30 × 0.22 × 0.17 | 0.18 × 0.15 × 0.08 |
| Crystal system | Triclinic | Monoclinic | Triclinic |
| Space group | P $\bar{1}$ | P2 ₁ /n | P $\bar{1}$ |
| a (Å) | 10.6474(17) | 11.0796(9) | 6.0051(3) |
| b (Å) | 10.7348(17) | 5.6102(5) | 8.7048(4) |
| c (Å) | 11.7927(19) | 13.8886(12) | 8.9090(4) |
| α (°) | 95.780(2) | 90.00 | 61.690(1) |
| β (°) | 115.148(2) | 99.3770(10) | 79.132(1) |
| γ (°) | 104.804(2) | 90.00 | 84.381(1) |
| V (Å ³) | 1145.4(3) | 851.76(13) | 402.63(3) |
| Z | 4 | 2 | 1 |
| ρ_{calc} (g/cm ³) | 1.463 | 1.7695 | 1.872 |
| F(000) | 528 | 462.8857 | 231 |
| $\mu_{\text{MoK}\alpha}$ (cm ⁻¹) | 0.116 | 1.339 | 2.470 |
| T (K) | 150(2) | 100.15 | 150(2) |
| Range of h, k, l | -14/14, -14/14, -16/16 | -14/14, -7/7, -18/18 | -7/7, -9/10, -10/10 |
| θ min/max | 1.965/29.183 | 2.19/28.46 | 2.858/34.89 |
| Reflections collected/unique/observed | 33,499/33,499/26,280 | 15,192/2153/1762 | 6620/1477/1461 |
| Data/restraints/parameters | 33,499/0/378 | 2153/0/134 | 1477/0/135 |
| Goodness-of-Fit (GOF) on F ² | 1.090 | 1.0367 | 1.095 |
| Final R indices [I > 2 σ (I)] | R ₁ = 0.0413 wR ₂ = 0.1119 | R ₁ = 0.0327 wR ₂ = 0.0905 | R ₁ = 0.0265 wR ₂ = 0.0698 |
| R indices (all data) | R ₁ = 0.0539 wR ₂ = 0.1172 | R ₁ = 0.0426 wR ₂ = 0.0947 | R ₁ = 0.0267 wR ₂ = 0.0700 |

were present in the unit cell of complex **C2**. The Cu(II) metal centre displayed a distorted octahedral geometry [$\angle \text{N}-\text{Cu}-\text{O} = 82.98(5)-97.02(5)^\circ$; $\angle \text{O}-\text{Cu}-\text{O} = 87.09(5)-92.91(5)^\circ$] wherein the equatorial positions were occupied by the nitrogen atom (1,2,4-triazole) and O atom (carboxylate) of two molecules of ligand **4**; the apical positions were coordinated by the water molecules (Fig. 3). The ligand **4**, retained its planarity in **C2**, which is revealed from the torsion angle between the aromatic ring (1,2,4-triazole and pyrimidine), and the carboxylate functionality ($\sim 5.05^\circ$). The N and O atom of the pyrimidine and carboxylate functionality, respectively, of the ligand molecule coordinated to the metal centre are involving hydrogen bonding via O–H...O and O–H...N interactions [$\text{O}-\text{H}\cdots\text{O} = 2.858(2)$ Å, $\angle \text{O}-\text{H}-\text{O} = 165^\circ$; $\text{O}-\text{H}\cdots\text{N} = 3.044(2)$ Å, $\angle \text{O}-\text{H}-\text{N} = 167^\circ$] with the metal bound water molecules, resulted in a

four member ring (square shaped) supramolecular hydrogen bonded synthon (Table 2). This square shaped synthon further expanded to form a 2D hydrogen bonded sheet, and these sheets are further packed into a three dimensional network structure via weak C–H...O hydrogen bonding.

2.5. Hirshfeld surface analysis

In order to understand and quantify the nature of intermolecular interactions in **C1** and **C2**, a Hirshfeld surface analysis was performed (Fig. 4). Possible supramolecular interactions with the neighbouring molecules are highlighted by conventional mapping of d_{norm} on molecular Hirshfeld surfaces. Hirshfeld surfaces of **C1** and **C2** are spotted with red and white colour indicating strong (strong proximity) and

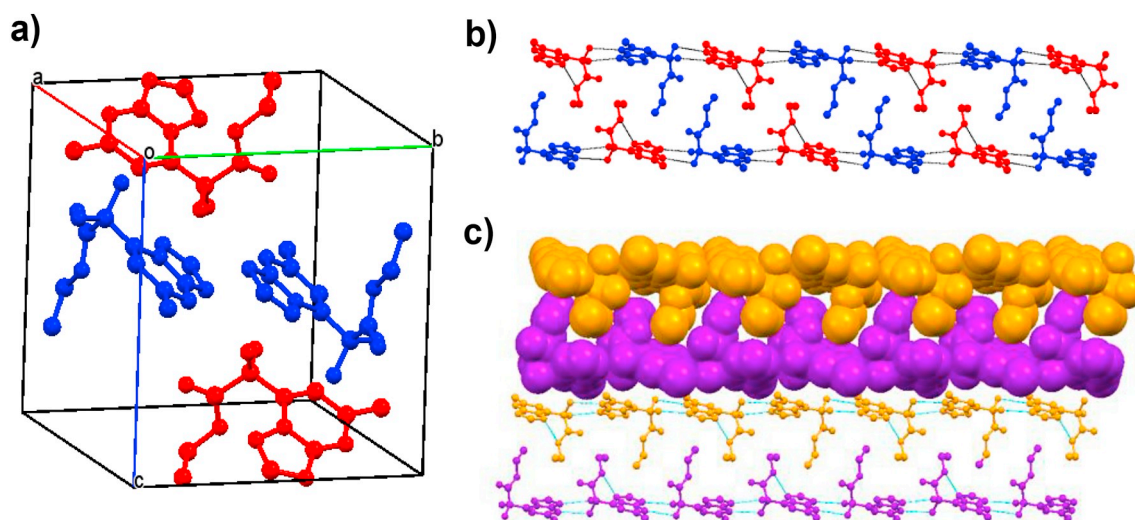


Fig. 1. View of the crystal of the intermediate product **5** – a) Packing of crystallographically independent molecules of **5** (shown in red and blue colour) within the triclinic unit cell; b) 1D hydrogen bonded chains and its parallel packing; c) self-assembly of the 1D chains via interdigitation of ester moieties; interacting chains are shown in purple and orange in an alternating fashion.

Table 2
Hydrogen bonding parameters for **5**, **C1** and **C2**.

| D–H...A | D–H (Å) | H...A (Å) | D...A (Å) | D–H...A (°) | Symmetry operation for A |
|--------------------|-----------|-----------|------------|-------------|---------------------------|
| C1 | | | | | |
| O(3)–H(3A)...O(2) | 0.870(2) | 2.018(2) | 2.868(2) | 165.37(18) | 2 – x, 2 – y, 1 – z |
| O(3)–H(3B)...N(3) | 0.870(2) | 2.059(2) | 2.924(2) | 173.2(2) | 3/2 – x, 1/2 + y, 1/2 – z |
| C(7)–H(7A)...O(2) | 0.980(9) | 2.472(10) | 3.422(3) | 163.4(8) | 1 – x, 2 – y, 1 – z |
| C2 | | | | | |
| O(3)–H(3A)...O(2) | 0.87 | 2.01 | 2.858(2) | 165 | –x, 1 – y, 1 – z |
| O(3)–H(3B)...N(1) | 0.87 | 2.19 | 3.044(2) | 167 | 1 – x, –y, 1 – z |
| C(6)–H(6)...O(3) | 0.95 | 2.51 | 3.439(2) | 165 | 1 + x, y, z |
| C(7)–H(7B)...O(1) | 0.98 | 2.45 | 3.425(3) | 177 | x, –1 + y, z |
| 4 | | | | | |
| O(1)–H(1A)...N(5) | 0.93(2) | 1.99(2) | 2.894(2) | 164(2) | 1 – x, –y, –z |
| O(2)–H(2A)...N(6) | 0.91(2) | 1.88(2) | 2.782(2) | 172.9(19) | 1 – x, –y, –z |
| O(5)–H(5A)...N(2) | 0.92(2) | 1.84(2) | 2.7593(19) | 179(3) | 1 – x, 1 – y, 1 – z |
| O(6)–H(6D)...O(7) | 0.91(2) | 2.38(2) | 2.7289(18) | 103.0(14) | x, y, z |
| O(6)–H(6D)...N(1) | 0.91(2) | 1.96(2) | 2.8346(18) | 162.5(19) | 1 – x, 1 – y, 1 – z |
| C(2)–H(2)...O(2) | 0.925(18) | 2.40(2) | 2.734(2) | 101.3(16) | x, y, z |
| C(5)–H(5)...N(3) | 0.98(2) | 2.56(2) | 3.383(3) | 140.8(14) | 2 – x, 1 – y, 1 – z |
| C(6)–H(6A)...O(2) | 0.98 | 2.54 | 3.382(2) | 145 | 1 – x, –y, 1 – z |
| C(15)–H(15)...O(7) | 0.98(2) | 2.39(2) | 3.218(3) | 141.9(16) | 1 – x, 1 – y, –z |

intermediate (or little proximity) hydrogen bonding interactions, respectively, between two atoms around the surface; and the blue colour shows no interactions. Strong hydrogen bonding interactions such as O–H...O and O–H...N in **C1** and **C2** involving metal bound water molecules, pyrimidine and carboxylate functionalities, can be seen in the Hirshfeld surface as red spots. The 2D fingerprint plot further revealed the quantification (percentage contribution) of various supra-molecular interactions in **C1** and **C2** (Figs. 4 and 5). In **C1**, the contribution of inter contacts to the Hirshfeld surfaces are O...H (24.9%),

N...H (14.8%), C...H (11.0%), and H...H (30.1%), and in **C2**, the interatomic contacts on the surface are O...H (27.1%), N...H (21.4%), C...H (8.4%), and H...H (25.9%). Interestingly, in **C1** and **C2**, there are two sharp spikes in the lower left area of the fingerprint plot, that belong to O–H...N ($d_i + d_e = 2.26$ and 2.28 , for **C1** and **C2** respectively) and O–H...O ($d_i + d_e = 2.41$ and 2.40 , for **C1** and **C2** respectively) interactions.

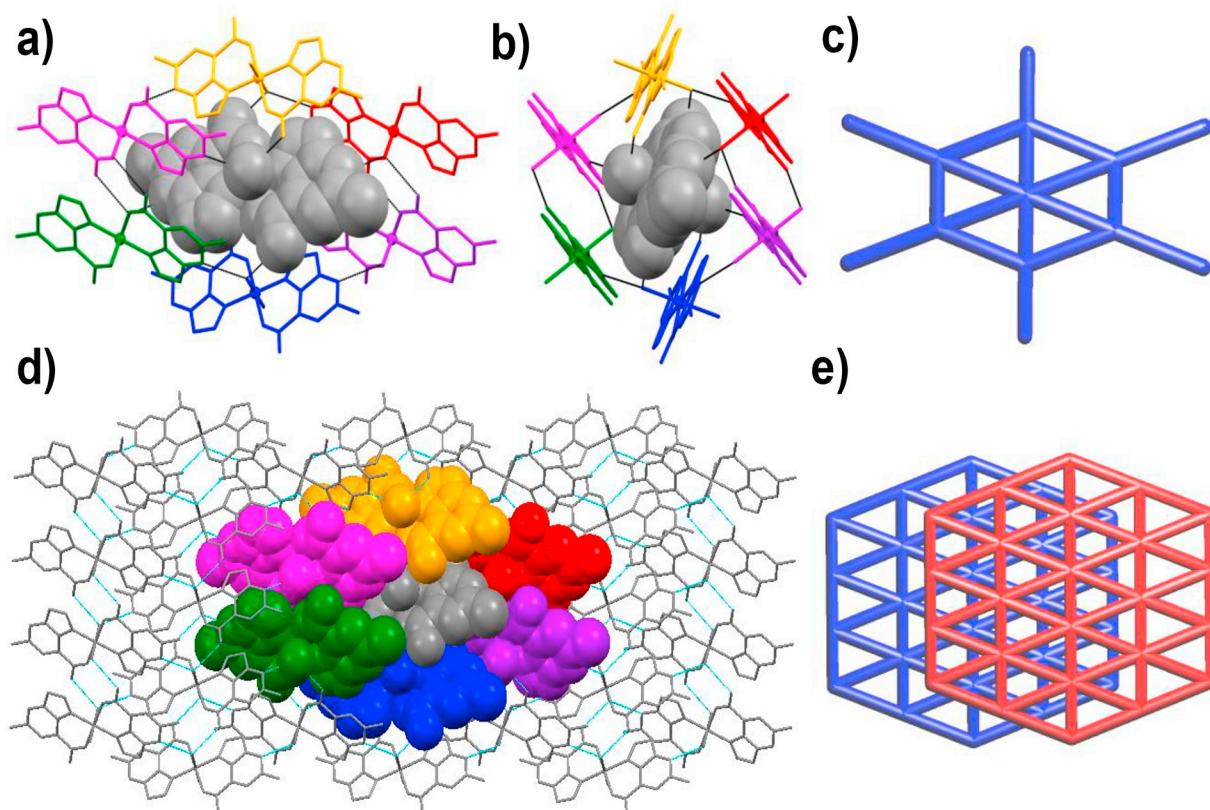


Fig. 2. Crystal structure illustration of **C1** – a) and b) primary supramolecular synthon formed by the hexagonal shaped self-assembly of six molecules of **C1** and a molecule at the centre of this hexagonal ring, in different views of crystallographic axis; c) TOPOS [47] view of the self-assembled primary supramolecular synthon; d) further self-assembly of supramolecular synthon into a 2D hydrogen bonded sheet mediated by O–H...O and O–H...N hydrogen bonding interactions (primary supramolecular synthon is shown in various colour and space fill model); e) TOPOS [48] view of the overall packing of 2D hydrogen bonded sheets.

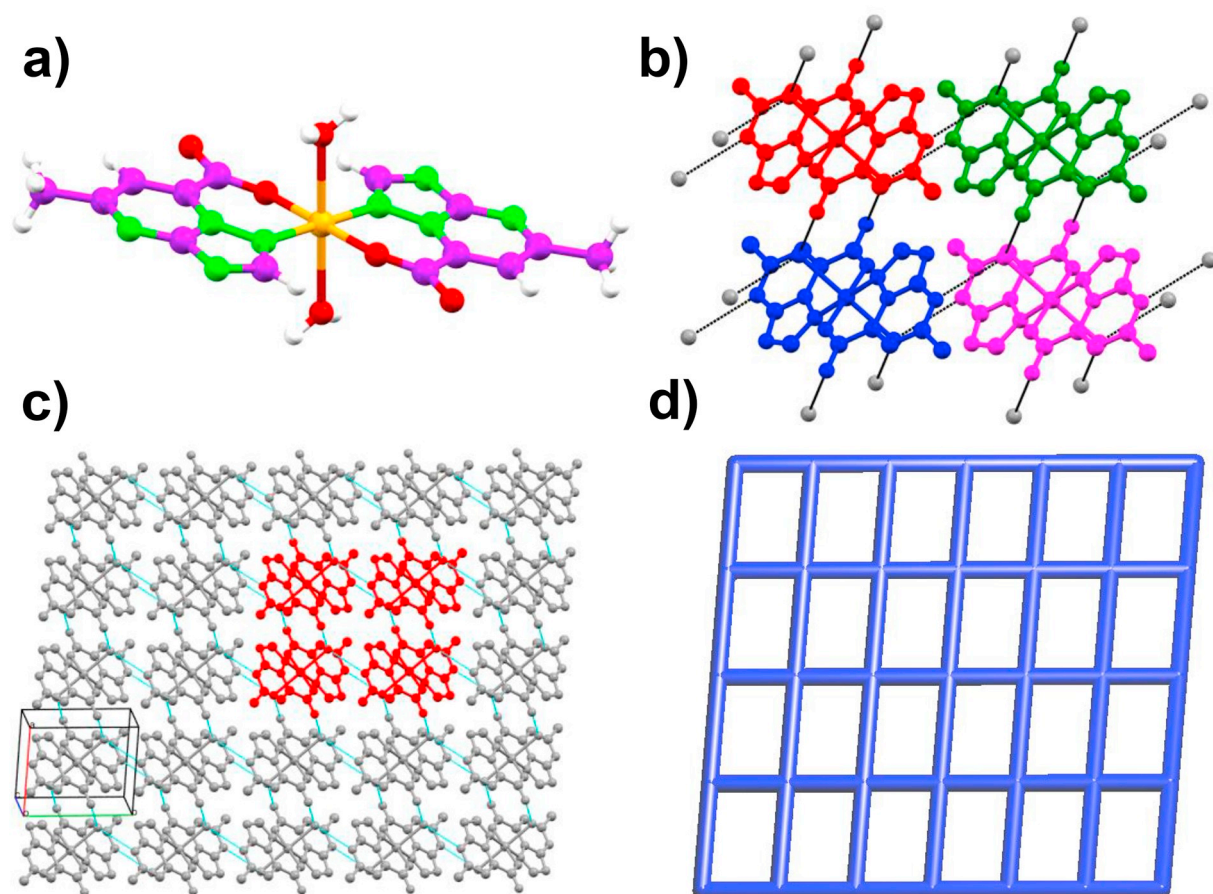


Fig. 3. View of the crystal structure of **C2** – a) crystal structure of **C2**, displaying the octahedral geometry of Cu(II) (colour code: C – purple, N – green, O – red, Cu(II) – orange, H – white); b) square shaped supramolecular hydrogen bonded synthon, formed by O–H...O and O–H...N interactions; c) further packing of this synthon into a 2D hydrogen bonded sheet (the square shaped synthon is shown in red colour); d) TOPOS view of the 2D hydrogen bonded sheet, displaying the square shaped primary supramolecular synthon.

2.6. ESI-MS

In order to confirm the structure of our two coordination complexes **C1** and **C2** (Scheme 3), we have firstly carried out a ESI-MS analysis. Normally, the expected protonated molecular ion would be $m/z = 454 [M+H]^+$. It is worthy to note that the Cu(II) ion in the complex is coordinated with two water molecules, as shown by single crystal X-ray diffraction (Figs. 1 and 2), which show deprotonation of two OH group of the ligand. Surprisingly, our ESI-MS analysis revealed a peak at $m/z = 418 [Cu(4)_2 + H]^+$ (Fig. S4, Appendix A), which corresponds to the complex missing two water molecules ($454 - 2 \times 18 = 418$ g/mol), as shown in Scheme S1 (Appendix A), for the dehydrated complex. A second peak was observed at $m/z = 440 [Cu(4)_2 + H + Na]^+$, which corresponds to the dehydrated protonated and sodiated complex. Subsequently, the energy was set to 20 eV, which yielded to a mass spectrum with a molecular ion peak at $m/z = 419$ (Fig. S5 in Appendix A), which corresponds to the dehydrated complex protonated twice: $[Cu(4)_2 + 2H]^+$.

Single crystals of **C1** and **C2** were then subjected to HRMS. The molecular ion was observed at $m/z = 465.36261$ which corresponds to $[Cu(4)_2 + 2H + 2Na]^+$ as shown in Figs. S7 and S8 (Appendix A). Thus, HRMS of our complexes did not show the molecular ion, but preferably derivated species.

2.7. Antioxidant activity

Recently, Cu(II) coordination complexes were explored as potential candidates for antioxidant activity determination [49]. Inspired by

these results, we have studied the antioxidant property of the compounds **5**, **L**, **C1** and **C2**. The antioxidant activity was systematically evaluated using three different assays at different concentration ranges. Free radical scavenging is one of the most known mechanism by which antioxidants inhibit oxidation and provide a simple, rapid, and sensitive procedure for screening the scavenging activity of radicals of specific compounds. The scavenger capacity is determined by measuring the decrease in the absorption of the 1,1-diphenyl-2-picrylhydrazyl acid (DPPH) and 2,2'-azino-bis (3-ethylbenzothiazoline-6 sulfonic acid (ABTS) radicals. Indeed, determination of DPPH · free radical scavenging activity is one of the most widely used methods for evaluating total antioxidant activity. The ability of synthesized compounds to reduce Fe^{3+} to Fe^{2+} by using the Ferric Reducing Antioxidant Power (FRAP) test was evaluated, and the results compared with that of standard antioxidants including the synthetic antioxidant dibutylhydroxytoluene (BHT), ascorbic acid and Trolox. These three assays are mostly used to measure the direct involvement of molecules into improving the primary antioxidant activity.

In this study, the tested compounds exhibited as certain degree of radical scavenging activity. Intermediate **5** and ligand **L** showed considerable activity with IC_{50} values of 29.87 ± 2.55 and 41.90 ± 2.55 μM , respectively, compared to BHT (IC_{50} of 19.06 μM). Complexes **C1** and **C2** exhibited however a lower DPPH scavenging capacity with IC_{50} values of 218.00 ± 1.42 and 286.90 ± 2.22 μM , respectively (Table 3).

The ABTS method is based on the ability of hydrogen or electron-donating antioxidants to decolorize the performed radical monocation of 2,2'-azino-bis (3-ethylbenzothiazoline-6-sulfonic acid) generated due

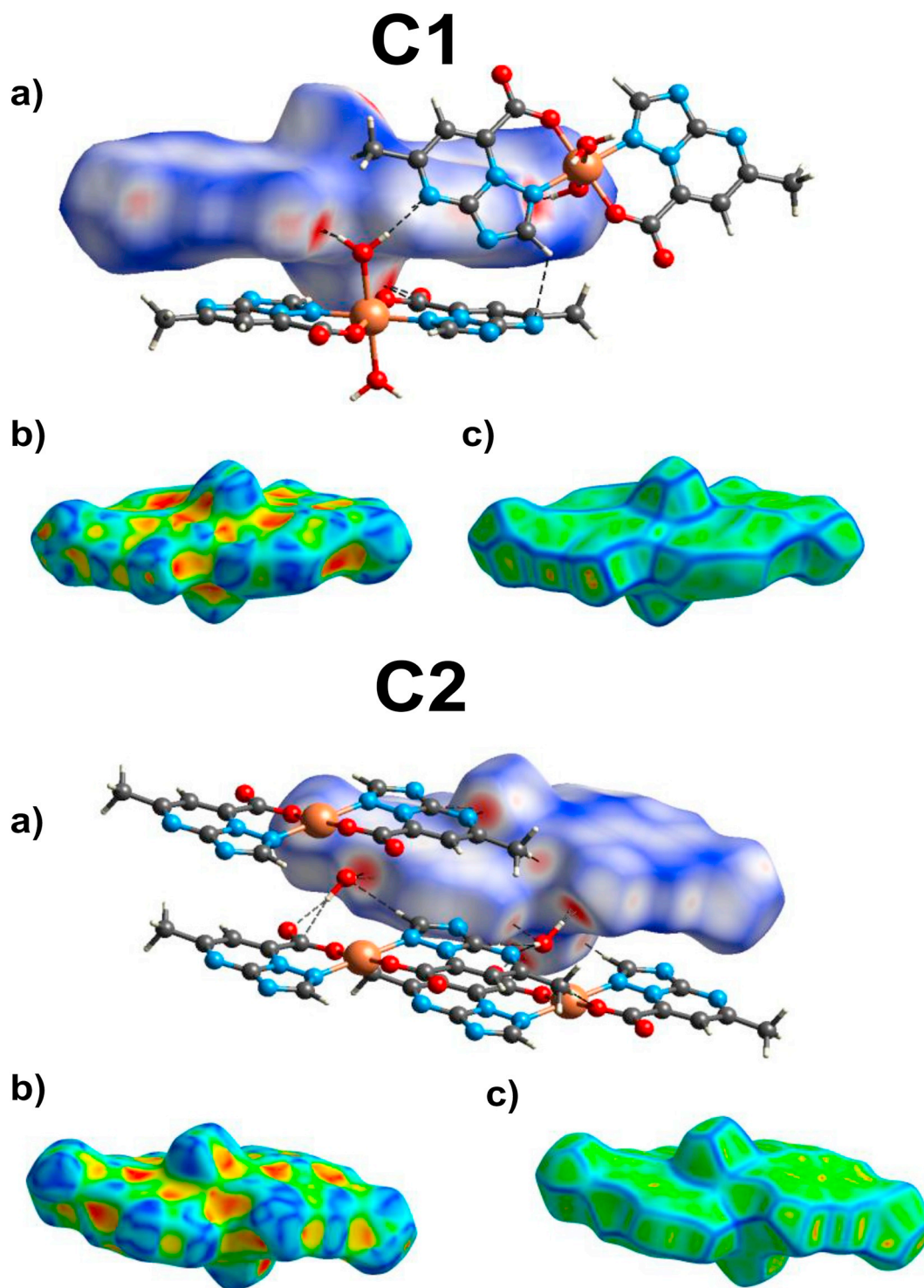


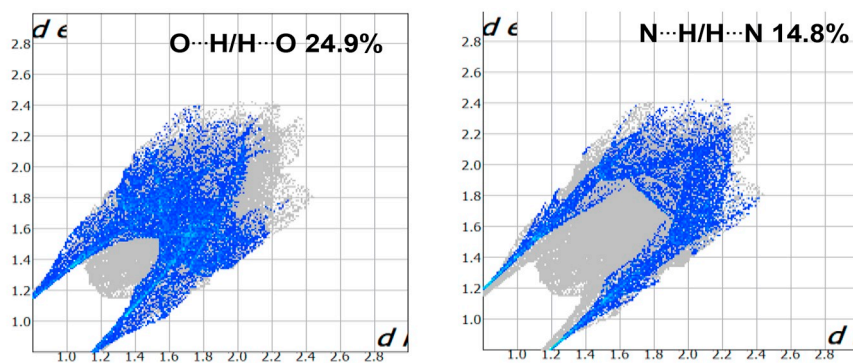
Fig. 4. a) Hirshfeld surface mapped with the d_{norm} function [colour code: red, white and blue colour represents strong, medium and least proximity for hydrogen bonding] of the C1 (top) and C2 (bottom). The interacting coordination complex is shown in “ball and stick” model; b) shape index of C1 (top) and C2 (bottom), displaying hydrogen bonding and stacking interactions (shown red and blue triangles). c) Curvedness of C1 (top) and C2 (bottom).

to oxidation of ABTS with potassium persulfate. When the ligands and their metal complexes were screened for their radical scavenging abilities towards this assay, **5** was found to have the best antioxidant activity with IC_{50} value of 53.21 μ M followed by the ligand (**L**) with IC_{50} value of 69.04 μ M. Complexes C1 and C2 had lower antioxidant activity in comparison (Table 3).

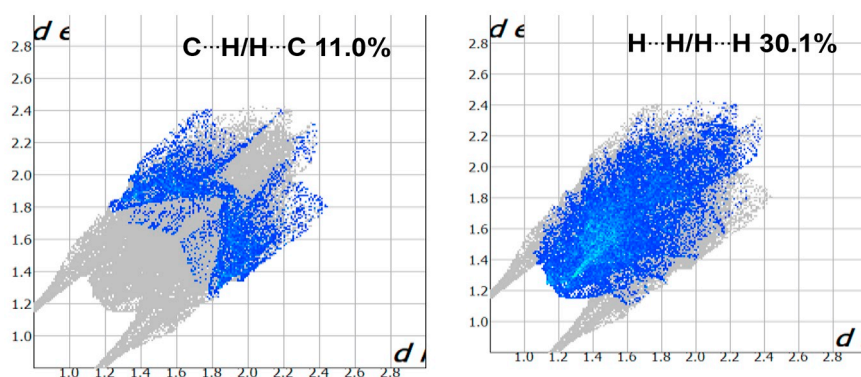
The reductive capabilities of ligand and its metal complex were assessed by the extent of reduction of ferricyanide into ferrocyanide.

The removal of the ligands and its metal complexes were studied at different concentrations, and were compared with ascorbic acid. As a result, the reducing capacity of the organic molecules **L** and **5** was greater than that of the metal complexes. The results of this experiment are in good agreement with the DPPH and ABTS tests.

C1



C1 - Total 100%



C2

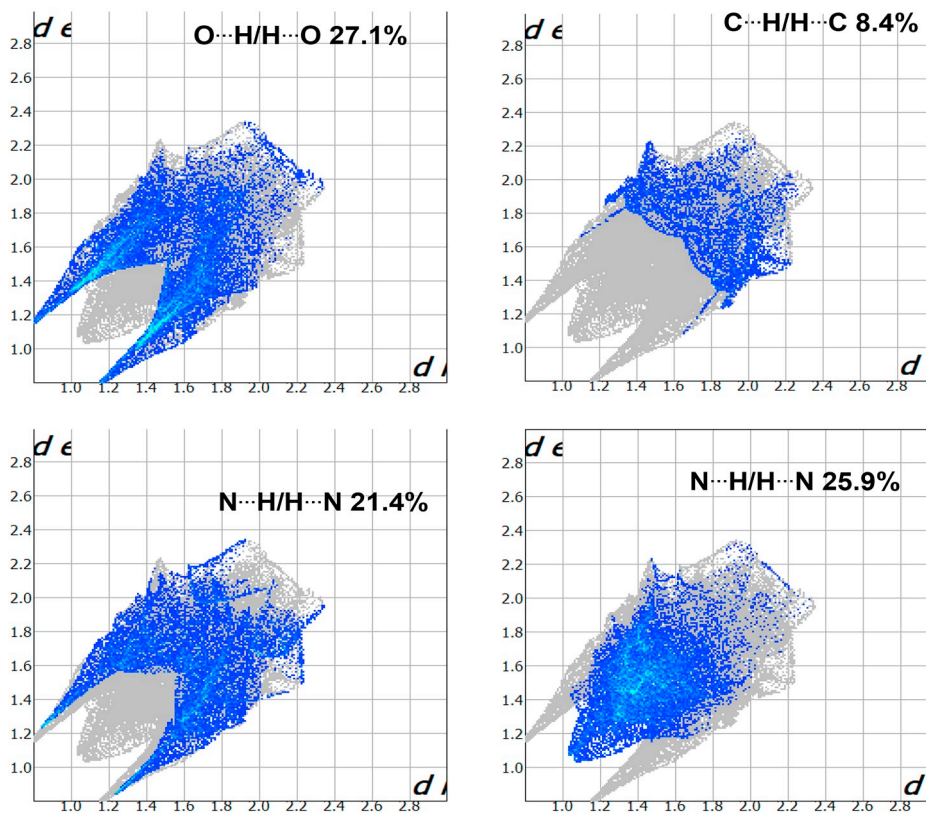


Fig. 5. 2D Fingerprint plots derived from Hirshfeld surfaces, displaying various intermolecular interactions for C1 (top) and C2 (bottom).

Table 3
Antioxidant activities of **L**, **5**, **C1** and **C2**.

| | DPPH | ABTS | FRAP |
|-----------|-----------------------|-----------------------|----------------|
| | IC ₅₀ (μM) | IC ₅₀ (μM) | μM EAA/mM comp |
| L | 41.90 ± 2.55 | 69.04 ± 1.66 | 73.3 ± 2.13 |
| C1 | 286.90 ± 2.22 | 144.6 ± 0.73 | 46.29 ± 1.91 |
| C2 | 218.00 ± 1.42 | 92.68 ± 2.07 | 54.18 ± 2.74 |
| 5 | 29.87 ± 2.55 | 53.21 ± 1.19 | 97.50 ± 3.19 |
| Standard | BHT = 19.06 ± 0.12 | Trolox = 7.71 ± 0.35 | – |

2.8. Effect of solvent in the formation of supramolecular polymorphs **C1** and **C2**

Supramolecular polymorphism [50] corresponds to the existence of organic or metal-organic molecules in more than one crystalline phase. As a result of this phenomenon, chemically identical molecules exhibit various packing arrangements in the solid state. The research in this area is currently in grooming stage, owing to their importance in academia and industry where crystallization is an attractive purification technique for pharmaceutically relevant compounds [51]. Moreover the bulk properties of all solid state crystalline materials fundamentally depend upon their supramolecular structures [52]. Thus, it is significant to study various factors which lead to supramolecular isomerism in organic or metal organic molecules. Such study is necessary to achieve more insights in the crystal engineering of molecules, and hence beneficial to create desired supramolecular structure. Solvent molecules (used for the crystallization of the compounds) play one of the crucial roles to induce supramolecular isomerism in coordination compounds [53]. In the present work, alcoholic solvents were introduced to induce the formation of supramolecular polymorphs **C1** (monoclinic, $P2_1/n$) and **C2** (triclinic, $P\bar{1}$). Both **C1** and **C2** were crystallized from exactly the same amounts of precursors materials (2:1 molar ratio of **4** and $\text{CuCl}_2 \cdot 2\text{H}_2\text{O}$) and for the same concentrations. The only difference is the solvent used for crystallization. EtOH and MeOH were used as the crystallizing solvents for **C1** and **C2**, respectively. It is worth mentioning that while we attempted to crystallize the Fe(II) coordination complex of **4**, no product could be obtained, contrary to Sabatino et al. who obtained an Fe(III) complex when reacting **4** with FeCl_3 [54]. We then thought to add a similar amount of Cu(II) to this solution which led to crystals of **C2**. The Fe(II) salt might have act as a template for the formation of **C2**, but further characterizations would be necessary to assess it. The supramolecular structures of **C1** and **C2** differ significantly from each other, even though both are chemically identical. Both supramolecular polymorphs **C1** and **C2**, packed strongly with the support of O–H...N, O–H...O, C–H...O hydrogen bonding interactions and lead to the formation of 2D hydrogen bonded sheet. The primary supramolecular synthon of **C1** and **C2**, located in this 2D hydrogen bonded sheet are hexagon and square shape architectures, involving six and four molecules, respectively. The difference in the packing of **C1** and **C2** is primarily due to the difference in the crystal system and space groups. Such difference is apparently influenced by the crystallization solvents. A molecular overlay diagram for **C1** and **C2**, with the Cu(II) atom, and other six atoms associated with the octahedral coordination acts as the common basis, is shown in Fig. 6. The torsion angle between the aromatic ring and the carboxylate functionality in **C1** and **C2** are $\sim 6.49\text{--}7.25^\circ$ and $\sim 5.05^\circ$, respectively. Moreover, the torsion angle between the metal coordinated ligand molecules of **4**, in **C1** and **C2** are 0° and 1.45° , respectively; meaning slight non planar conformation of ligand is present in the crystal structure of **C2**. We believe that due to this slight nonplanar structure of ligand and presence of more number of C–H...O interactions in **C2**, than that of **C1**, is the reason behind its more antioxidant activity compared to **C1**.

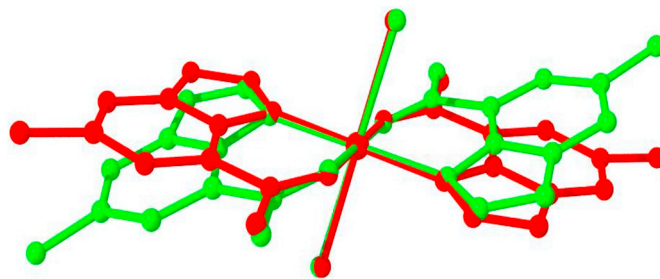


Fig. 6. A molecular overlay of the $[\text{Cu}(\mathbf{4})_2(\text{H}_2\text{O})_2]$ unit from **C1** (red) and **C2** (green), with the Cu(II), O atoms of water molecules, N and O atoms of the ligand **L1**, as the common basis.

3. Experimental

3.1. Synthetic procedures

7-Ethoxycarbonylmethyl-5-methyl-1,2,4-triazolo[1,5-*a*]pyrimidine (**L**) was synthesized according to a procedure previously described starting from 3-amino-1,2,4-triazole and 4-hydroxy-6-methyl-2-pyrrone [35–37]. Yield: 66%; $^1\text{H NMR}$ (CDCl_3) δ (ppm): 8,15 (s, 1H, H-2), 6,86 (s, 1H, H-6), 2,46 (s, 3H, CH_3), 4,39 (s, 2H, CH_2); 3,98 (s, 2H, CH_2); 1,02 (t, 3H, $\text{CH}_2\text{--CH}_3$). $^{13}\text{C NMR}$ (CDCl_3) δ (ppm): 166,60 (C=O); 164,71 (C-5), 154,84 (C-2), 154,74 (C-3a); 142,12 (C-7), 111,38 (C-6), 61,50 ($\text{CH}_2\text{--O}$), 35,71 ($\text{CH}_2\text{--7}$), 13,63 ($\text{CH}_3\text{--CH}_2$). HRMS ESI-MS (MeOH): $m/z = 221$ $[\text{M} + \text{H}]^+$.

$[\text{Cu}(\mathbf{4})_2(\text{H}_2\text{O})_2]$ (**C1**): To a solution of 0.25 mmol (55 mg) of **L** in ethanol (10 mL) was added slowly and with stirring a solution of $\text{CuCl}_2 \cdot 2\text{H}_2\text{O}$ (21.5 mg) in ethanol (5 mL) in a 2:1 molar ratio. The mixture was heated slightly, and then left under slow evaporation at r. t. After 48 h, blue single crystals were isolated. Yield: 57%. ESI-MS (MeOH): $m/z = 418$ $[\text{Cu}(\mathbf{4})_2 + \text{H}]^+$, 440 $[\text{Cu}(\mathbf{4})_2 + \text{H} + \text{Na}]^+$.

$[\text{Cu}(\mathbf{4})_2(\text{H}_2\text{O})_2]$ (**C2**): To a solution of 0.25 mmol (55 mg) of **L** in methanol (10 mL) was added slowly and with stirring a solution of 0.125 mmol (25 mg) of $\text{FeCl}_2 \cdot 4\text{H}_2\text{O}$ in methanol (5 mL). The mixture was heated slightly, a solution of $\text{CuCl}_2 \cdot 2\text{H}_2\text{O}$ (21.4 mg) in ethanol (5 mL) was added slowly, and then leaves under slow evaporation at room temperature. After 72 h, blue single crystals were isolated. Yield: 45%. ESI-MS (MeOH): $m/z = 418$ $[\text{Cu}(\mathbf{4})_2 + \text{H}]^+$, 440 $[\text{Cu}(\mathbf{4})_2 + \text{H} + \text{Na}]^+$.

The two complexes **C1** and **C2** are very stable in air as confirmed by XRD analyses carried out after overseas shipping in the United States. Analyses by ESI-MS and HRMS of **C1** and **C2** systematically revealed the loss of two coordinated water molecules, due to the strong effect of the electric field.

Intermediate (**5**): To a solution of 0.92 mmol of **L** (202.4 mg) in ethanol (35 mL) was added slowly and with stirring a solution of $\text{MnCl}_2 \cdot 4\text{H}_2\text{O}$ (95 mg) in ethanol (15 mL). The mixture was heated slightly, and then abandoned for slow evaporation at room temperature. After 48 h, a precipitate was isolated and then re-crystallized from methanol (20 mL). After two weeks of slow evaporation at room temperature, colourless single crystals of ethyl 2,2-

dihydroxy-2-(5-methyl-[1,2,4]triazolo[1,5-*a*]pyrimidin-7-yl)acetate (**5**) were isolated (56%). ¹H NMR (300 MHz, DMSO-*d*₆) δ (ppm): 0.98 (t, 3H, CH₃), 2.69 (s, 3H, CH₃), 4.06 (q, 2H, CH₂), 7.45 (s, 2H, 2OH), 7.89 (s, 1H, CH-Ar), 8.55 (s, 1H, CH-Ar). ¹³C NMR (75 MHz, DMSO-*d*₆) δ (ppm): 14.27 (CH₃), 25.51 (Ar-CH₃), 61.79 (CH₂), 90.99 (C(OH)₂), 108.35 (CH-Ar), 149.06 (2N=C-N), 155.59 (C=N), 166.25 (=C-N), 168.57 (C=O).

3.2. Materials and methods

Chemical reagents were purchased from Fluka, Sigma and Aldrich chemicals. Melting points were measured using a Büchi B-545 digital capillary melting point apparatus and used without correction. Organic reactions were controlled by TLC using aluminium sheets with silica gel 60 F254 available from Merck. IR spectra were recorded on a Perkin-Elmer VERTEX 70 FT-IR spectrometer covering the vibrational range 400–4000 cm⁻¹. ¹H and ¹³C NMR spectra were recorded in DMSO-*d*₆ or CDCl₃ on a Bruker spectrometer (300 MHz). Chemical shifts are expressed in ppm using tetramethylsilane (TMS) as internal reference. Mass spectra were recorded on a LCQ Advantage Thermo Electron apparatus with a TOF analyzer. High resolution mass spectrometry (HRMS) was recorded on a Q-Exactive orbitrap from Thermo Fisher. Positive ESI was used as ionization mode.

3.3. Crystallography

X-ray single-crystal data were collected on single crystals using Mo Kα (λ = 0.7107 Å) radiation on a Bruker SMART APEX diffractometer equipped with a CCD area detector. Unit cell refinement data reduction (SAINT) and structure solution as well as refinement (SHELXL) [55] were carried out using the software package of SMART APEX. The crystal structures were solved by direct methods and refined in a routine manner. In all the three structures, non-hydrogen atoms were treated anisotropically. For complexes **C1** and **C2**, the hydrogen atoms were geometrically fixed. On the other hand in the crystal structure of **5**, some of the possible hydrogen atoms were located on a difference Fourier map and refined, and the other hydrogen atoms were geometrically fixed. Molecular graphics were generated using MERCURY 3.9 [56] and POV-Ray softwares. The details of crystallographic data and the structure solution as well as the refinement are given in Table 1. CCDC 1915469, 1915467 and 1915468 contain the supplementary crystallographic data for **5**, **C1** and **C2**, respectively, and can be obtained free of charge from the Cambridge Crystallographic Data Centre via www.ccdc.cam.ac.uk/data_request/cif.

3.4. Hirshfeld surface analysis

Hirshfeld surface analysis and the corresponding 2D fingerprint plots of **5**, **C1** and **C2** were determined by using the software CRYSTAL EXPLORER 3.1 [57]. We have used the following equation to calculate the normalized contact distance (d_{norm}), from the values of d_e (distance between the Hirshfeld surface and external molecule), d_i (distance between the Hirshfeld surface and inside molecule) and Van der Waals radii of the atoms (r_i^{vdw} or r_e^{vdw}). We can easily determine the regions of the compound which participate to the intermolecular interactions. From the following equation, we can calculate the normalized contact distance (d_{norm}), from the values of d_e (distance between the Hirshfeld surface and external molecule), d_i (distance between the Hirshfeld surface and inside molecule) and Van der Waals radii of the atoms (r_i^{vdw} or r_e^{vdw}).

$$d_{norm} = \frac{d_i - r_i^{vdw}}{r_i^{vdw}} + \frac{d_e - r_e^{vdw}}{r_e^{vdw}}$$

3.5. Antioxidant activity

3.5.1. DPPH radical scavenging activity

The radical-scavenging activity of **L**, **5**, **C1** and **C2** were evaluated vs. the stable 1,1-diphenyl-2-picrylhydrazyl acid (DPPH) radical, according to the method described by Li et al. [58] In this procedure, 2 mL of a 4% solution of DPPH in methanol (w/v) was mixed with 500 μL of sample solutions at different concentrations (15–1500 μM). The scavenging capacity was determined spectrophotometrically after 30 min of incubation by monitoring the decrease of the absorbance at λ = 517 nm. Lower absorbance of the reaction mixture indicates higher free radical scavenging activity. Ascorbic acid was used as standard. The percent DPPH scavenging effect was calculated using the following equation:

$$\% \text{of scavenging} = [(A_c - A_t)/A_c] \times 100$$

where A_c is the absorbance of the control sample (DPPH solution without test sample) and A_t is the absorbance of the test sample (DPPH solution + test compound). Tests were performed in triplicate, and the results averaged.

3.6. ABTS radical scavenging activity

The ABTS (2,2'-azino-bis (3-ethylbenzothiazoline-6 sulfonic acid) free radical-scavenging activity of **L**, **5**, **C1** and **C2** was estimated using the method described by Tuberoso et al. [59] The blue-green ABTS radical cation was produced by reaction between 7 mM ABTS and 70 mM potassium persulfate in water. The mixture was stored at room temperature in the darkness for 16 h prior use. The ABTS solution was then diluted with 80% MeOH to obtain an absorbance of 0.700 ± 0.005 at λ = 734 nm. One hundred microliters of sample solutions at different concentrations (125–2000 μM) were added to 2 mL of ABTS solution and the absorbance was recorded at λ = 734 nm after 1 min incubation at room temperature. This was compared to the blank where 200 μL of the methanol was added to 2 mL of ABTS solution. A standard curve was obtained by using a 3,4-dihydro-6-hydroxy-2,5,7,8-tétraméthyl-2H-1-benzopyran-2-carboxylic acid (Trolox) reference solution at various concentrations. The scavenging activities of different concentrations of synthesized compounds against ABTS radical were also measured to calculate the IC₅₀, and the procedure was similar to the DPPH scavenging method described above. The test was carried out in triplicate and IC₅₀ values were reported as means ± SD.

$$\% \text{Inhibition} = (A_c - A_t/A_c)/100$$

where A_c is the absorbance of the control, and A_t is the absorbance in the presence of the samples or reference. The control did not contain compound or standard.

3.6.1. Ferric reducing/antioxidant power (FRAP) assay

The ferric-reducing capacity of the ligands and complexes was investigated by using the potassium ferricyanide-ferric chloride method with some modifications [60]. Briefly, the sample (1 mL) at 1 mM was mixed with 2.5 mL of phosphate buffer (0.2 M, pH = 6.6) and 2.5 mL of 1% K₃[Fe(CN)₆]. The mixture was then incubated at 50 °C for 20 min to reduce ferricyanide into ferrocyanide. A portion (2.5 mL) of trichloroacetic acid (10%) was added to the mixture which was then centrifuged at 3000 rpm for 10 min. Finally, 2.5 mL of the supernatant was mixed with 2.5 mL of distilled water and 0.5 mL of a FeCl₃ solution (0.1%, w/v), and the absorbance was measured at λ = 700 nm. Increased absorbance values indicate a higher reducing power. The results were expressed as ascorbic acid equivalent per gram of product dry weight (μM AAE/mM comp).

4. Conclusions

The present study involved the synthesis of two Cu(II) complexes

crystallized as supramolecular isomorphs (**C1** and **C2**), obtained as a result of 7-ethoxycarbonylmethyl-5-methyl-1,2,4[1,5-a]pyrimidine (**L**) reaction with $\text{CuCl}_2 \cdot 2\text{H}_2\text{O}$. The reaction involves an intermediate ethyl 2,2-dihydroxy-2-(5-methyl-1,2,4-triazolo[1,5-a]pyrimidin-7-yl)acetate (**5**) which has been isolated and structurally characterized. Interestingly **C1** and **C2** turned out to be 2D hydrogen bonded structures, as a result of their supramolecular assembly. However the primary supramolecular synthon in **C1** and **C2** are a six membered ring, and a square shaped hydrogen bonded architecture, respectively, supported by $\text{O}-\text{H}\cdots\text{O}$ and $\text{O}-\text{H}\cdots\text{N}$ hydrogen bonding interactions, involving metal bound water molecules, pyrimidine and carboxylate moieties. Hirshfeld surface analysis of these complexes, further revealed that these coordination complexes are stabilized by the presence of various supramolecular interactions sustained by various functionalities. In addition, the antioxidant properties of these molecules were evaluated in vitro revealing a higher activity for **C2** compared to **C1** as supported by X-ray crystallography.

Declaration of competing interest

There is no conflict of interest to declare.

Acknowledgements

This work was supported by a bilateral WBI action with Morocco (COP 22 Program 2018-2022) and the Fonds de la Recherche Scientifique-FNRS (CDR 33694457).

Appendix A. Supplementary data

Supplementary data to this article can be found online at <https://doi.org/10.1016/j.jinorgbio.2020.111092>.

References

- [1] O. Augusto, S. Miyamoto, Principles of Free Radical Biomedicine, vol. 1, Nova Publishers, 2011, p. 19.
- [2] M. Valko, D. Leibfritz, J. Moncol, M.T.D. Cronin, M. Mazur, Int. J. Biochem. Cell Biol. 39 (2007) 44.
- [3] P.D. Ray, B.-W. Huang, Y. Tsuji, Cell. Signal. 24 (2012) 981.
- [4] E. Songül, Ş. Musa, Ö. Mustafa, R. Apak, B. Ülküseven, Inorg. Chim. Acta 469 (2018) 495.
- [5] G. Nirmala, R. Aveli, V. Narendrula, S.D. Shivaraj, J. Mol. Struct. 1173 (2018) 173.
- [6] K. Chkirate, S. Fattach, K. Karrouchi, N.K. Sebbar, E.M. Essassi, J.T. Mague, S. Radi, M.A. Faouzi, N.N. Adarsh, Y. Garcia, J. Inorg. Biochem. 191 (2019) 21.
- [7] I. Łakomska, M. Fandzloch, Coord. Chem. Rev. 327 (2016) 221.
- [8] J.M. Salas, M.A. Romero, M.P. Sánchez, M. Quirós, Coord. Chem. Rev. 193 (1999) 1119.
- [9] A.M. Gamal-Eldeen, N.A. Hamdy, H.A. Abdel-Aziz, E.A. El-Hussieny, I.M. Fakhr, Eur. J. Med. Chem. 77 (2014) 323.
- [10] S. Massari, G. Nannetti, J. Desantis, G. Muratore, S. Sabatini, G. Manfroni, A. Loregian, J. Med. Chem. 58 (2015) 3830.
- [11] B. Huang, C. Li, W. Chen, T. Liu, M. Yu, L. Fu, J. Balzarini, Eur. J. Med. Chem. 92 (2015) 754.
- [12] S.L. Deev, M.V. Yasko, I.L. Karpenko, A.N. Korovina, A.L. Khandazhinskaya, V.L. Andronova, G.A. Galegov, T.S. Shestakova, E.N. Ulomskii, V.L. Rusinov, O.N. Chupakhin, M.K. Kukhanova, Bioorg. Chem. 38 (2010) 265.
- [13] M. Kannan, A.V. Raichurkar, F.R.N. Khan, P.S. Iyer, Bioorg. Med. Chem. Lett. 25 (2015) 1100.
- [14] M. Rodriguez-Torres, E.M. Yoshida, P. Marcellin, S. Srinivasan, V.S. Purohit, C. Wang, J.L. Hammond, Ann. Hepatol. 13 (2014) 364.
- [15] E.R. da Silva, N. Boechat, L.C. Pinheiro, M.M. Bastos, C.C. Costa, J.C. Bartholomeu, T.H. da Costa, Chem. Biol. Drug Des. 86 (2015) 969.
- [16] H. Wang, M. Lee, Z. Peng, B. Blázquez, E. Lastochkin, M. Kumarasiri, S. Mobashery, J. Med. Chem. 58 (2015) 4194.
- [17] Q. Chen, X.L. Zhu, L.L. Jiang, Z.M. Liu, G.F. Yang, Eur. J. Med. Chem. 43 (2008) 595.
- [18] H.M. Ashour, O.G. Shaaban, O.H. Rizk, I.M. El-Ashmawy, Eur. J. Med. Chem. 62 (2013) 341.
- [19] T. Saito, T. Obitsu, C. Minamoto, T. Sugiura, N. Matsumura, S. Ueno, M. Toda, Bioorg. Med. Chem. 19 (2011) 5955.
- [20] G. Fischer, Adv. Heterocycl. Chem. 57 (1993) 81.
- [21] G. Fischer, Adv. Heterocycl. Chem. 95 (2007) 143–219.
- [22] J.M. Méndez-Arriaga, I. Oyarzabal, G. Escolano, A. Rodríguez-Diéguez, M. Sánchez-Moreno, J.M. Salas, J. Inorg. Biochem. 180 (2018) 26.
- [23] J. Ruiz, M.D. Villa, N. Cutillas, G. López, C.D. Haro, D. Bautista, L. Valencia, Inorg. Chem. 47 (2008) 4490.
- [24] I. Ramírez-Macias, C. Marín, J.M. Salas, A. Caballero, M.J. Rosales, N. Villegas, M. Sánchez-Moreno, J. Antimicrob. Chemother. 66 (2011) 813.
- [25] I. Łakomska, K. Hoffmann, A. Wojtczak, J. Sitkowski, E. Maj, J. Wietrzyk, J. Inorg. Biochem. 141 (2014) 188.
- [26] W.T. Monte, W.A. Kleschick, R.W. Meikle, S.W. Snider, J. Bordner, J. Heterocyclic Chem. 26 (1989) 1393.
- [27] J. Reiter, L. Pongó, P. Dyortsák, Tetrahedron 43 (1987) 2497.
- [28] M.A. Shaban, A.Z. Nasr, Adv. Heterocycl. Chem. 49 (1990) 277.
- [29] J.G. Haasnoot, T. Favre, F. Loek W. Hinrichs, J. Reedijk, Angew. Chem. 100 (1988) 884.
- [30] A.T.H. Lenstra, B.H.J. Slot, P.T. Beurskens, J.G. Haasnoot, J. Reedijk, Recl. Trav. Chim. Pays-Bas. 108 (1989) 133.
- [31] A.H. Velders, L. Pazderski, F. Uguzzoli, M. Biagini-Cingi, A.M. Manotti-Lanfredi, J.G. Haasnoot, J. Reedijk, Inorg. Chim. Acta 273 (1998) 259.
- [32] I. Łakomska, H. Kooijman, A.L. Spek, W.Z. Shen, J. Reedijk, Dalton Trans. (48) (2009) 10736.
- [33] A.B. Caballero, C. Marín, I. Ramirez-Macias, A. Rodriguez-Dieguez, M. Quiros, J.M. Salas, M. Sanchez-Moreno, Polyhedron 33 (2012) 137.
- [34] A.B. Caballero, A. Rodriguez-Dieguez, M. Quiros, J.M. Salas, O. Huertas, I. Ramirez-Macias, F. Olmo, C. Marín, G. Chaves-Lemaur, R. Gutierrez-Sanchez, M. Sanchez-Moreno, Eur. J. Med. Chem. 85 (2014) 526.
- [35] B. Elotmani, M. El Mahi, E.M. Essassi, C. R. Chim. 5 (2002) 517.
- [36] M. Fettuouhi, A. Boukhari, B. Elotmani, E.M. Essassi, Acta Cryst C52 (1996) 1031.
- [37] S. Lahmidi, N.K. Sebbar, T. Hokelek, K. Chkirate, J.T. Mague, E.M. Essassi, Acta Cryst E74 (2018) 1833.
- [38] K. Chkirate, S. Kansiz, K. Karrouchi, J.T. Mague, N. Dege, E.M. Essassi, Acta Cryst E75 (2019) 154.
- [39] K. Chkirate, S. Kansiz, K. Karrouchi, J.T. Mague, N. Dege, E.M. Essassi, Acta Cryst E75 (2019) 33.
- [40] S. Lahmidi, M. El Hafi, M. Boulhaoua, A. Ejjoummany, M. El Jemli, E.M. Essassi, J.T. Mague, J. Mol. Struct. 1177 (2019) 131.
- [41] K. Chkirate, K. Karrouchi, N. Dege, N.K. Sebbar, A. Ejjoummany, S. Radi, N.N. Adarsh, A. Talbaoui, M. Ferbinteanu, E.M. Essassi, Y. Garcia, New J. Chem. 44 (2020) 2210–2221.
- [42] H. Sterckx, J. De Houwer, C. Mensch, W. Herrebout, K.A. Tehrani, B.U. Maes, Beilstein J. Org. Chem. 12 (2016) 144–153.
- [43] F.M. Moghaddam, Z. Mirjafary, H. Saeidian, M.J. Javan, Synlett (2008) 892–896.
- [44] B. El Azzaoui, J. Fifani, E.M. Tjiou, E. Essassi, J. Jaud, L. Lopez, J. Bellan, Tetrahedron Lett. 40 (1999) 4677–4680.
- [45] R.P. Bell, A.O. McDougall, Trans. Farad. Soc. 56 (1960) 1281.
- [46] F.Y. Liu, D.-M. Zhou, X.-L. Zhao, J.-F. Kou, Acta Cryst C73 (2017) 1010.
- [47] S. Radi, A. Yahyi, A. Ettouhami, A.C. Jha, N.N. Adarsh, K. Robeyns, Y. Garcia, Polyhedron 85 (2015) 383.
- [48] V.A. Blatov, A.P. Shevchenko, D.M. Proerpio, Cryst. Growth Des 14 (7) (2014) 3576–3586.
- [49] L. Esmaili, M.G. Perez, M. Jafari, J. Paquin, P. Ispas-Szabo, V. Pop, M. Andruh, J. Byers, M.A. Mateescu, J. Inorg. Biochem. 192 (2019) 87.
- [50] B. Moulton, M.J. Zaworotko, Chem. Rev. 101 (2001) 1629–1658.
- [51] B. Rodríguez-Spong, C.P. Price, A. Jayasankar, A.J. Matzger, N. Rodríguez-Hornedo, Adv. Drug Deliv. Rev. 56 (2004) 241–274.
- [52] a J.-M. Lehn, Supramolecular Chemistry Concepts and Perspectives, VCH, Weinheim, Germany, 1995; b G.R. Desiraju, Nature 412 (2001) 397.
- [53] D.K. Kumar, A. Das, P. Dastidar, Crystal Growth Des. 7 (2007) 2096–2105.
- [54] P. Sabatino, S. D'Agostino, J. Isopi, S. Rubino, M. Marcaccio, M.A. Girasolo, Polyhedron 162 (2019) 45–51.
- [55] G.M. Sheldrick, Acta Cryst. C 71 (2015) 3.
- [56] C.F. Macrae, P.R. Edgington, P. McCabe, E. Pidcock, G.P. Shields, R. Taylor, M. Towler, J. Van De Streek, J. Appl. Crystallogr. 39 (2006) 453.
- [57] S.K. Wolff, D.J. Grimwood, J.J. McKinnon, M.J. Turner, D. Jayatilaka, M.A. Spackman, CrystalExplorer 3.1, Univ. Western Australia, Crawley, Australia, 2013.
- [58] T. Li, S. Li, Y. Dong, R. Zhu, Y. Liu, Food Chem. 145 (2014) 335.
- [59] M. Tuberoso, E. Boban, D. Bifulco, F.M.P. Budimir, Food Chem. 140 (2013) 686.
- [60] M. Oyaizu, Jpn. J. Nutr. Diet. 44 (1986) 307.